

Octopus-like Reaching Motion: A Perspective Inspired by Whipping

Shengyao Zhang[†], Yiyuan Zhang^{†,*}, *Graduate Student Member, IEEE*, Chenrui Zhang, *Member, IEEE*, Yiming Li, Wenci Xin, *Graduate Student Member, IEEE*, Yuliang Liufu, Hong Wei Ng, and Cecilia Laschi, *Fellow, IEEE*

Abstract—The stereotypical reaching motion of the octopus arm has drawn growing attention for its efficient control of a highly deformable body. Previous studies suggest that its characteristic bend propagation may share underlying principles with the dynamics of a whip. This work investigates whether whip-like passive dynamics in water can reproduce the kinematic features observed in biological reaching and their similarities and differences. Platform-based whipping tests were performed in water and air while systematically varying material stiffness and driving speed. Image-based quantification revealed that the Ecoflex Gel 2 arm driven at 150 rpm (motor speed) reproduced curvature propagation similar to that observed in octopus reaching. However, its bend-point velocity decreased monotonically rather than exhibiting the biological bell-shaped profile, confirming that the octopus reaching movement is not merely a passive whipping behavior. The absence of propagation in air further highlights the critical role of the surrounding medium in forming octopus-like reaching motion. This study provides a new perspective for understand biological reaching movement, and offers a potential platform for future hydrodynamic research.

I. INTRODUCTION

The reaching movement of the octopus arm exemplifies one of the most stereotyped and simplified control strategies in its highly deformable muscular system. Unlike the human arm with a limited number of joints, the octopus arm possesses virtually infinite degrees of freedom, functioning as a muscular hydrostat capable of bending, elongating, shortening, and twisting without skeletal support. Despite this structural complexity, octopuses can extend their arms toward a target through highly similar reaching movements, following a consistent bend-propagation pattern that is organized both spatially and temporally [1]–[3].

Previous studies have suggested that this movement shares intriguing parallels with whipping-like passive dynamics [1], [2], [5], [6]. Biological reaching can be described as a base-to-tip propagating bend wave—arising from continuous neural drive together with intrinsic elasticity and hydrodynamic interaction—in which a traveling front of stiffening

[†]These authors contributed equally to this work.

*Corresponding author: Yiyuan Zhang (yiyuan.zhang@u.nus.edu)

Department of Mechanical Engineering, National University of Singapore, Singapore 117575, Singapore.

This work was supported by the following projects: the DESTRO project (“Dextrous, strong yet soft robots,” R2210IR124), funded by MAE (Italy) and A*STAR (Singapore); the REBOT project (“Rethinking underwater robot manipulation,” Moe-t2eP50221-0010), funded by the Singapore Ministry of Education; and the RoboLife project (“Soft robots with morphological adaptation and life-like abilities”), funded by the NUS Funding Agency (Singapore). The authors also would like to thank Wanlin Huang for help with final result visualization.

and muscle activation produces curvature and energy transmission [7], [8] reminiscent of a whip crack, as shown in Figure. 1a [4]. The analogy suggests that the octopus may utilize passive mechanical whipping to achieve rapid, efficient reaching movement, converting local activation into

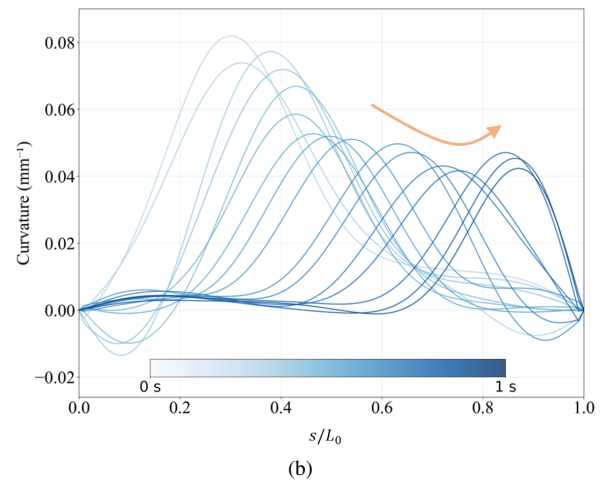
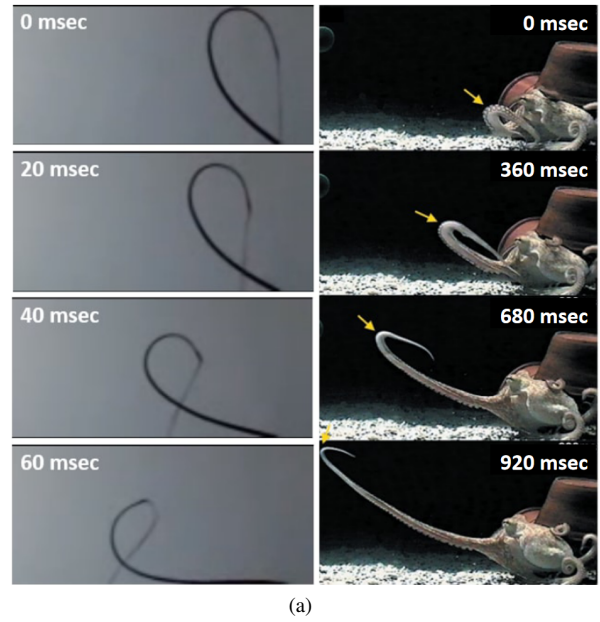


Fig. 1. (a) Multiple exposures of a bullwhip exhibiting propagating waves during motion, kinematically similar to an octopus arm. [4] (b) Curvature pattern of real octopus reaching behavior (s/L_0 denotes the normalized arc length along the arm, with s being the arc-length coordinate and L_0 the undeformed arm length).

a large-scale sweeping-like reaching motion.

The detailed kinematics of the octopus reaching behavior reveal several invariant features across individuals and contexts. The motion is initiated by the formation of a localized bend near the arm base, which then propagates distally along a nearly planar trajectory, maintaining a constant-curvature bend propagation region over a significant portion of the movement, as shown in Figure. 1b [1], [3], [7]. The bend-point velocity shows a characteristic bell-shaped temporal profile with smooth acceleration and deceleration, implying that control is exerted chiefly over the bend's spatiotemporal position rather than over discrete muscle segments [1]. Biomechanical and computational models further demonstrate that a simple traveling wave of muscle stiffening can reproduce the experimentally observed velocity profiles and curvature evolutions [3], [7], supporting the notion that the system relies on local passive wave mechanics to generate globally coordinated motion. Collectively, these findings portray octopus reaching as a dynamic balance between active control and passive mechanical propagation, embodying principles that resonate strongly with whipping dynamics—where a localized deformation evolves into a smooth, accelerating wave culminating in effective, directed motion.

The whipping motion represents a canonical example of energy focusing and curvature propagation in flexible continua. When an impulse is applied to the handle of a whip, a traveling loop or curvature wave propagates toward the free end, gradually accelerating as the whip's radius tapers and mass per unit length decreases [9]. This process converts distributed elastic and kinetic energy into a concentrated, high-velocity motion at the tip—eventually reaching supersonic speed and producing the characteristic crack. Theoretical analyses based on elastic rod models reveal that the traveling wave maintains a quasi-constant curvature while local velocity increases, consistent with conservation of energy and momentum in a homogeneous medium. Importantly, this bend propagation mechanism is not unique to whips; similar dynamic principles have been identified in biological systems such as fly-fishing lines, flagella, and even octopus arms, where a local curvature travels through the body to produce directed motion. From this perspective, the octopus reaching behavior may be hypothesized as a biological manifestation of the whipping phenomenon [4]. Both systems rely on the propagation of a localized bend—maintaining nearly constant curvature and exhibiting a bell-shaped velocity evolution. In whips, the traveling loop is a fully passive mechanical wave driven by the initial impulse and geometric tapering; in octopus arms, a similar propagation arises from the coupling of muscle activation waves and passive environmental interactions. These parallels suggest that understanding whipping dynamics provides not only a physical analogue but also an experimental framework for interpreting the passive wave-based control strategy observed in octopus reaching motions.

Building upon these findings, we aimed to examine whether the whipping dynamics in a fluid environment could

reproduce the bend-propagation characteristics observed in octopus reaching, and whether such motions would exhibit kinematic features comparable to biological reaching movements. In particular, this study explores whether a whip-like passive motion, when performed underwater, can generate bend propagation, curvature evolution, and bend-point velocity profiles similar to those recorded in octopus reaching movements.

We first performed hand-driven trials in water to mimic octopus reaching movements and then used the captured trajectories to reverse design a repeatable rig: a PLA+ 3D-printed frame carrying a tapered silicone arm that can reproduce the motions under controlled settings. Using this device, we executed repeated runs while systematically switching silicone grades and adjusting the rotation rate to examine how these factors shape the outcome.

The videos were processed with a dedicated pipeline: frames were uniformly sampled, the midline was reconstructed for each frame, and from this we derived curvature evolution and bend-point speed, which were compared with published biological data. An Ecoflex Gel 2 (abbreviated as Gel 2) arm operated at 150 rpm (motor speed) produced the closest match in curvature propagation to octopus reaching; however, the bend-point speed declined steadily rather than forming the bell-shaped time course typical of animals. Under identical actuation in air, no propagation was observed, underscoring the dominance of the fluid environment. Collectively, these results verify that the biological reaching movement is not merely an arm-whipping motion from a robotics perspective, highlight the importance of environment in shaping the reaching behavior, and provide a simple yet insightful experimental framework that may serve as a tool for future hydrodynamics research on reaching movements.

II. METHOD

A. Design of Mechanism

We first conducted manual whipping experiments in an underwater environment to qualitatively reproduce the reaching motion observed in octopus arms, as shown in Figure. 2. As the extracted midline of real octopus reaching movement and manual whipping motion shown in Figure. 3a and Figure. 3b, the resulting motion sequence exhibited a distinct bend propagation pattern similar to the biological reaching behavior. Subsequently, a motion tracking software (Tracker) was used to extract the positional coordinates and orientation angles of the silicone arm's base movement, as presented in Figure. 3c. The recorded data were plotted on an x-y coordinate system and imported into MotionGen, where a virtual mechanism capable of outputting an analogous trajectory was generated, as shown in Figure. 3d. Based on the generated trajectory, the detailed structure of the linkage mechanism was designed in SolidWorks, including each connecting link, joint, and gear configuration (see Figure. 3e). To overcome the inherent limitation of the motor's output torque, an additional set of power-amplifying gears was incorporated to enhance energy transmission efficiency. Due to the constraints of manual

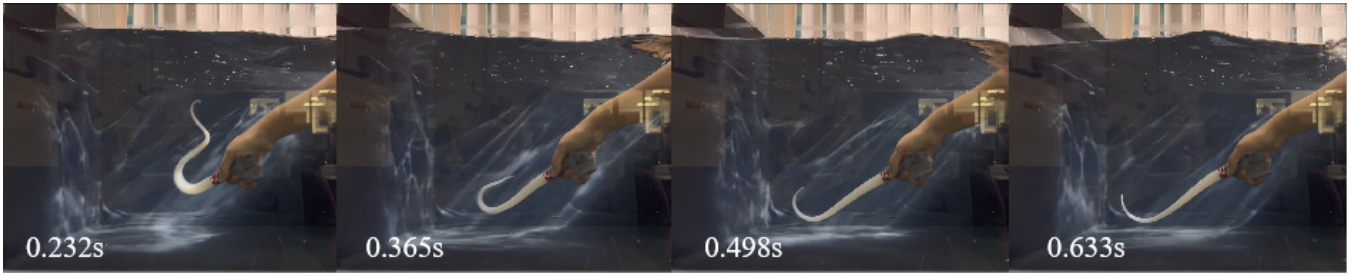


Fig. 2. Underwater manual whipping motion.

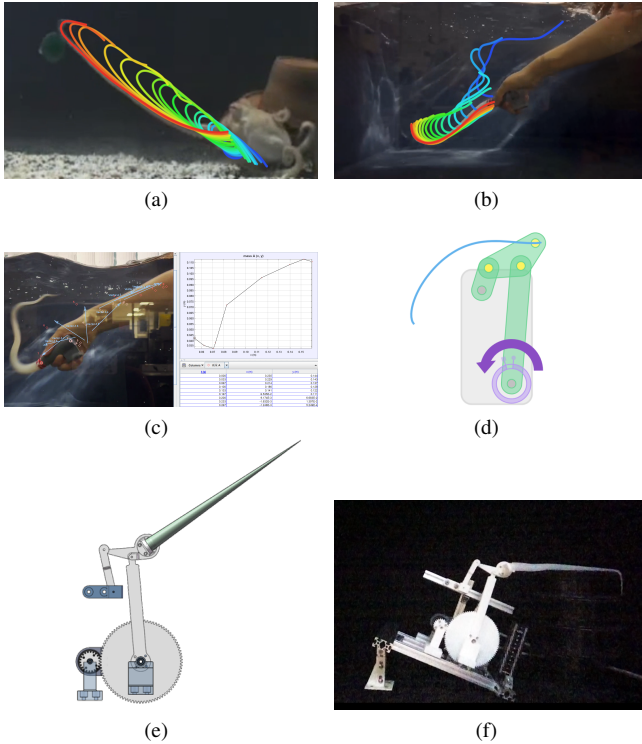


Fig. 3. (a) The trajectory of the midline shift during the octopus's reaching motion. (b) The trajectory of the midline shift during underwater manual whipping motion. (c) Position and orientation extraction in Tracker. (d) Mechanisms generation in MotionGen. (e) SolidWorks Model. (f) Physical prototype of the mechanism.

manipulation within the water tank, the observed motion primarily exhibited a diagonally downward wave propagation. To better approximate the actual reaching kinematics of the octopus—where the curvature wave propagates nearly along a horizontal plane—we elevated a section of the mechanism's supporting frame by approximately 20 degrees clockwise. This adjustment redirected the path of motion transmission in a nearly horizontal direction, allowing a more biologically consistent wave propagation pattern.

Finally, all parts were fabricated using 3D printing with PLA+ material and subsequently assembled into a complete prototype mechanism with a tapered silicone arm, as shown in Figure. 3f and the motor used in the mechanism has a KV value of 350 rpm/V, a maximum current of 15 A, and a maximum power of 300 W. The resulting system provided

a compact platform that allows fine-tuning of geometric and actuation parameters for future experiments on wave dynamics and underwater performance.

B. Data Extraction

Midline Extraction. To quantitatively analyze the deformation of the silicone octopus arm, we developed a custom image-processing pipeline. As shown in Figure. 4a, each video frame was first processed with Meta's Segment Anything Model 2 (SAM 2) [10] to segment the moving arm from the underwater background. A binary mask was then applied to remove the rigid supporting structure, yielding a clean extraction of the silicone arm (Figure. 4b). The extracted region was skeletonized to obtain its medial axis (Figure. 4c). Because skeletonization can occasionally introduce spurious branches, all branch points were detected and removed. The three terminal nodes of the remaining skeleton were subsequently identified, and the two closest endpoints (E_2, E_3) were used to compute their midpoint M , which served as an auxiliary node to reconstruct the main, ordered centerline (Figure. 4d).

Curvature Computation. The reconstructed midline was smoothed and uniformly resampled to generate evenly spaced reference points along the arm. For each sampled point,

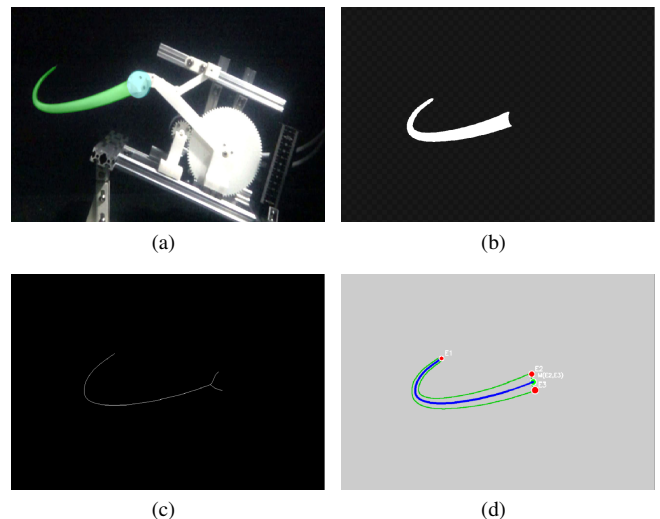


Fig. 4. (a) Segmentation on original image. (b) Extracted mask. (c) Original midline with a branch. (d) Final midline.

the local curvature κ was computed using a three-point geometric method: for a point P_i and its two adjacent neighbors P_{i-1} and P_{i+1} , a circle passing through these three points was fitted, and the curvature was defined as

$$\kappa = \frac{1}{R}, \quad (1)$$

where R is the radius of the fitted circle. This approach yields a continuous curvature profile along the arm, effectively describing the spatial propagation of bending.

Bend-point Velocity Identification. The bending point was defined as the midline location with the minimum x -coordinate in each frame. Using the known time interval between consecutive frames, the displacement of this bending point was tracked to compute its velocity. This procedure provides a quantitative measure of the propagation speed of the curvature wave along the soft robotic arm during the reaching motion.

III. RESULTS

During the initial manual whipping tests, the Gel 2 arm demonstrated the most distinct and similar bending response among all tested materials. Based on this observation, we selected Gel 2 as the reference material for subsequent variable-speed experiments, aiming to determine an appropriate driving velocity capable of generating clear bend propagation. After identifying this optimal condition, the same fixed-speed tests were conducted for the other two materials (Ecoflex 10 and Dragonskin 10) for comparison.

In the variable-speed tests, three driving motor velocities were evaluated: 30 rpm, 90 rpm, and 150 rpm. Motions

exceeding 210 rpm were excluded because the arm exhibited out-of-plane deviations that disrupted the planar curvature propagation. For each condition, the recorded trajectories were processed to visualize the bend point velocity as a function of normalized time and velocity and the temporal evolution of curvature along the normalized arm length, as shown in Figure. 6b and Figure. 7.

For different driving speeds of the Gel 2 arm (Figure. 7a–7c), the curvature pattern at 150 rpm was most consistent with biological reaching (see Figure. 5), showing a temporal evolution similar to that observed in octopus arm motion (Figure. 1b). The curvature first decreased, then increased, and finally decayed, resulting in the largest amplitude and most distinct propagation among the samples tested. In contrast, Ecoflex 10 and Dragonskin 10 produced smaller curvature magnitudes and less continuous propagation (Figure. 7c–7e).

In both the variable-speed experiments (Gel 2 at 30, 60, and 150 rpm) and the variable-material experiments (Gel 2, Ecoflex 10, and Dragonskin 10 at a fixed speed of 150 rpm), the propagation velocity of the bend point along the x -direction exhibited a monotonically decreasing trend over time (Figure. 6b). In all cases, the bend point started with a relatively high velocity, which rapidly decayed and gradually approached zero.

IV. DISCUSSION

Material and speed strongly modulate the bend propagation. Among the tested conditions, Gel 2 generated the largest curvature amplitudes and the most continuous transmission; Ecoflex 10 showed intermediate behavior, while Dragonskin

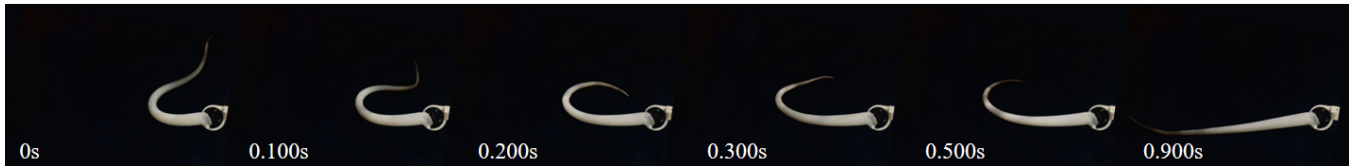
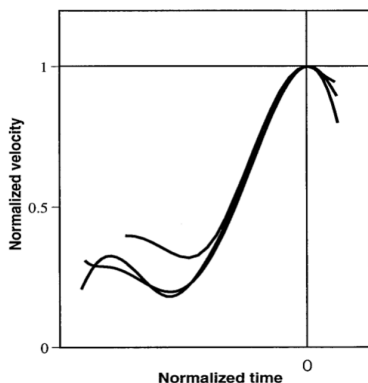
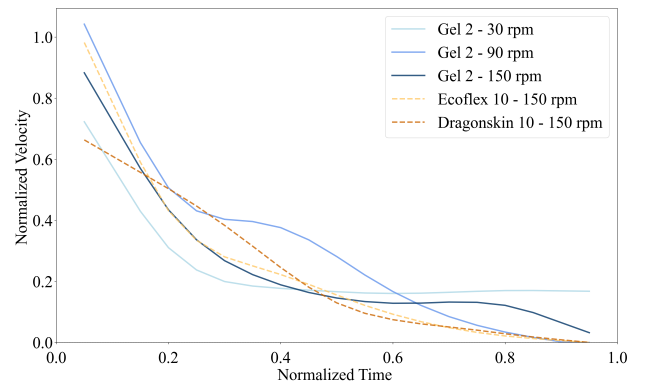


Fig. 5. Ecoflex Gel 2 underwater performance at 150 rpm.

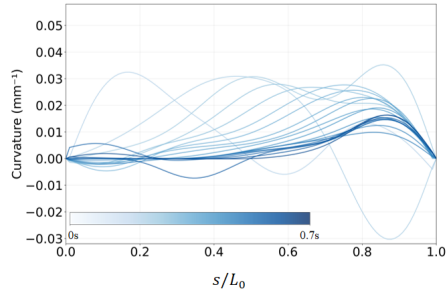


(a) Normalized velocity pattern for velocity and distance and aligned at the peaks. [1]

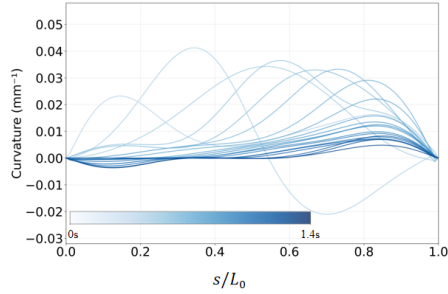


(b) Normalized velocity pattern in the experiment.

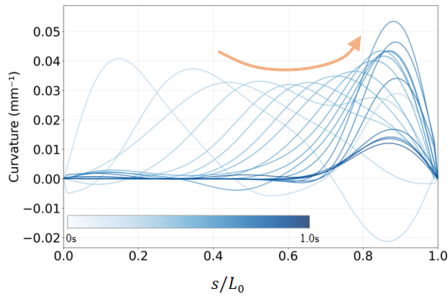
Fig. 6. Curvature and bend point velocity characteristics of bend propagation.



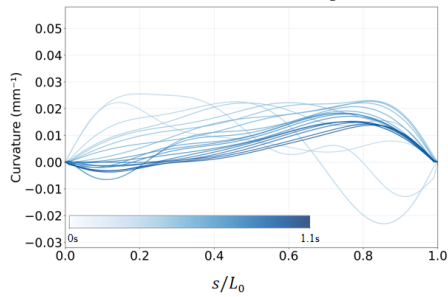
(a) Ecoflex Gel 2 at 30 rpm



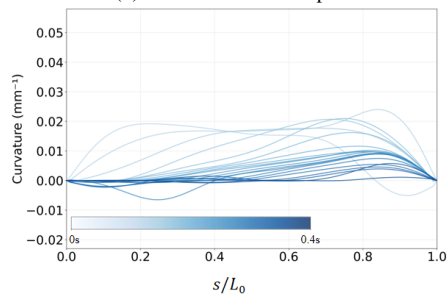
(b) Ecoflex Gel 2 at 90 rpm



(c) Ecoflex Gel 2 at 150 rpm



(d) Ecoflex 10 at 150 rpm



(e) Dragonskin 10 at 150 rpm

Fig. 7. Curvature characteristics of bend propagation under different driving speeds and materials.

10 attenuated fastest. Driving at 150 rpm provided an optimal balance between input energy and hydrodynamic loading, producing the most similar propagation to biological reaching. By contrast, lower speeds yielded insufficient momentum to sustain wave transmission, whereas excessive driving speeds introduced inertial and hydrodynamic instabilities that disrupted the planar mode of propagation.

Despite the clear spatial resemblance between the curvature evolution of Gel 2 at 150 rpm and biological reaching, the bend-point velocity shows a monotonically decreasing time course in both the variable-speed and variable-material experiments (see Figure. 6b) instead of the bell-shaped profile typical of biological reaching as shown in Figure. 6a. This finding supports the interpretation that the observed motion represents a passive hydrodynamic propagation rather than an actively controlled reaching behavior. Mechanistically, the monotonic decay accords with dissipative propagation of a passive wave, where viscous drag from the fluid continuously drain energy: the initial actuation originates at the base and attenuates as it travels, leading to a reduction of kinetic energy and curvature amplitude.

Interestingly, the curvature patterns of Gel 2 at low driving speed (30 rpm) exhibited temporal profiles similar to those of Ecoflex 10 and Dragonskin 10 driven at 150 rpm. This correspondence suggests that curvature propagation depends not only on material modulus but also on the relative balance between actuation intensity and inertial loading. The softer Gel 2 at low driving speed and the stiffer Ecoflex 10 and Dragonskin 10 at moderate speed appear to reach comparable dynamic regimes where elastic recovery dominates over inertia-driven momentum transfer. Under these conditions, the bending wave travels through passive redistribution of kinetic and elastic energy along the arm, leading to similar curvature attenuation profiles across materials. This behavior aligns with the whip-wave dynamics described by McMillen and Goriely [9], where energy imparted at the base propagates through a continuous medium via inertial coupling and geometric nonlinearity.

Furthermore, at higher speeds (210 rpm), the silicone arm occasionally exhibited non-planar motion characterized by twisting and asymmetric trajectories. We hypothesize that this phenomenon arises from strong fluid–structure coupling, where the interaction between the rapidly deforming arm and the surrounding flow generates three-dimensional hydrodynamic instabilities. Similar out-of-plane deformations have been reported in previous fluid–structure interaction studies of flexible bodies in oscillatory or traveling-wave motion [11], [12]. In these works, the coupling between structural elasticity, inertial loading, and unsteady vortex shedding can drive spontaneous transitions from planar to helical or chaotic motion once the driving velocity exceeds a critical threshold. In our system, this transition likely reflects the onset of such coupling-induced instability, suggesting that fluid feedback becomes dynamically significant beyond the regime of quasi-planar propagation.

These findings indicate that the bend propagation observed in our experiments can be parsimoniously explained by a

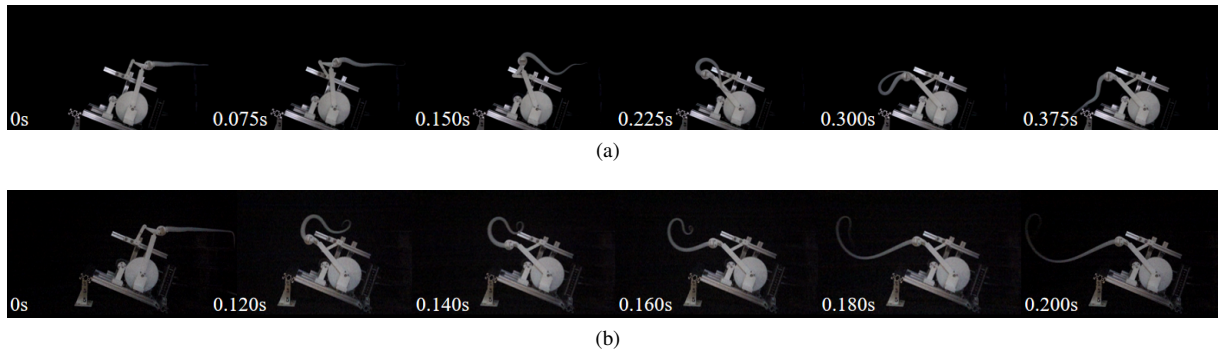


Fig. 8. Ecoflex Gel 2 performance in air at (a) 150 rpm (b) 330 rpm.

passive hydrodynamic mechanism. Once a local bend is initiated near the base, distributed drag from the surrounding water effectively suppresses the unactuated portions of the arm and advects the bend distally along a nearly planar path. The absence of propagation in air under identical conditions (Gel 2 driven at 150 rpm), as shown in Figure. 8a, further supports this interpretation. In addition, experiments in the attached video conducted in air with driving speeds at 210, 270, and 330 rpm (see Figure. 8b) revealed bend propagation patterns that differed substantially from those observed in biological reaching, accompanied by a marked increase in bend-point velocity [9]. This suggests that, in the absence of fluid-mediated damping and added-mass effects, the motion is dominated by direct mechanical inertia rather than hydrodynamic coupling. Therefore, we speculate that the surrounding fluid plays an important role in shaping curvature propagation, consistent with previous biological findings describing passive wave transmission in “non-activated” octopus arm segments [3].

V. CONCLUSIONS

This study examined whip-like motions in a fluid environment and showed that, while the Gel 2 arm driven at 150 rpm reproduces a curvature evolution that resembles octopus reaching, the bend-point velocity decays monotonically and therefore does not exhibit the bell-shaped temporal profile characteristic of biological reaching. Together with the absence of bend propagation in air, these findings indicate that the observed propagation is dominated by buoyancy, passive hydrodynamics and fluid–structure interactions. In this sense, our results offer a complementary perspective on why reaching is not a simple whipping behavior.

Beyond this conceptual point, our experiments reveal how material properties and driving speed bound the envelope of curvature propagation, with Gel 2 and 150 rpm offering the most biological like spatial propagation among the tested conditions. The methodology—combining controlled actuation, underwater trials, and quantitative curvature and velocity analyses—provides a simple and reproducible platform for quantitative, reaching-like kinematic studies. We anticipate that this platform can support deeper hydrodynamics research on reaching movements, including systematic studies of medium viscosity, arm geometry, and input shaping.

Future work will explore drive profiles and stiffness distributions aimed at approaching bell-shaped velocity histories without sacrificing propagation robustness, and extend the analysis to 3D kinematics at higher speeds.

REFERENCES

- [1] Y. Gutfreund, T. Flash, Y. Yarom, G. Fiorito, I. Segev, and B. Hochner, “Organization of octopus arm movements: a model system for studying the control of flexible arms,” *Journal of Neuroscience*, vol. 16, no. 22, pp. 7297–7307, 1996.
- [2] G. Sumbre, Y. Gutfreund, G. Fiorito, T. Flash, and B. Hochner, “Control of octopus arm extension by a peripheral motor program,” *Science*, vol. 293, no. 5536, pp. 1845–1848, 2001.
- [3] Y. Yekutieli, R. Sagiv-Zohar, R. Aharonov, Y. Engel, B. Hochner, and T. Flash, “Dynamic model of the octopus arm. i. biomechanics of the octopus reaching movement,” *Journal of neurophysiology*, vol. 94, no. 2, pp. 1443–1458, 2005.
- [4] A. C. Noel, “Grip, grab, and groom: The biomechanics of frog and cat tongues,” Ph.D. dissertation, Georgia Institute of Technology, 2018.
- [5] Y. Gutfreund, T. Flash, G. Fiorito, and B. Hochner, “Patterns of arm muscle activation involved in octopus reaching movements,” *Journal of Neuroscience*, vol. 18, no. 15, pp. 5976–5987, Aug 1998. [Online]. Available: <https://www.jneurosci.org/content/18/15/5976>
- [6] J. Alupay, J. Mather, and K. Iskarous, “A syntactic analysis of a complex motor action: the octopus arm ‘slap,’” *Marine Biology*, vol. 170, no. 99, p. –, Jun 2023. [Online]. Available: <https://doi.org/10.1007/s00227-023-04243-y>
- [7] I. Zelman, M. Titon, Y. Yekutieli, S. Hanassy, B. Hochner, and T. Flash, “Kinematic decomposition and classification of octopus arm movements,” *Frontiers in computational neuroscience*, vol. 7, p. 60, 2013.
- [8] T. Wang, U. Halder, E. Gribkova, M. Gazzola, and P. G. Mehta, “Control-oriented modeling of bend propagation in an octopus arm,” in *2022 American Control Conference (ACC)*. IEEE, 2022, pp. 1359–1366.
- [9] T. McMillen and A. Goriely, “Whip waves,” *Physica D: nonlinear phenomena*, vol. 184, no. 1-4, pp. 192–225, 2003.
- [10] N. Ravi, V. Gabeur, Y.-T. Hu, R. Hu, C. Ryali, T. Ma, H. Khedr, R. Rädle, C. Rolland, L. Gustafson, E. Mintun, J. Pan, K. V. Alwala, N. Carion, C.-Y. Wu, R. Girshick, P. Dollár, and C. Feichtenhofer, “Sam 2: Segment anything in images and videos,” *arXiv preprint arXiv:2408.00714*, 2024. [Online]. Available: <https://arxiv.org/abs/2408.00714>
- [11] J.-s. Wang, D. Fan, and K. Lin, “A review on flow-induced vibration of offshore circular cylinders,” *Journal of Hydrodynamics*, vol. 32, no. 3, pp. 415–440, 2020.
- [12] L. Ma, K. Lin, D. Fan, J. Wang, and M. S. Triantafyllou, “Flexible cylinder flow-induced vibration,” *Physics of Fluids*, vol. 34, no. 1, 2022.